GaSb superluminescent diodes with broadband emission at 2.55 μm

Nouman Zia,[a] Jukka Viheriälä, Eero Koivusalo, Heikki Virtanen, Antti Aho, Soile Suomalainen, and Mircea Guina
Optoelectronics Research Centre, Tampere University of Technology, Tampere FIN-33101, Finland

(Received 15 November 2017; accepted 18 January 2018; published online 30 January 2018)

We report the development of superluminescent diodes (SLDs) emitting mW-level output power in a broad spectrum centered at a wavelength of 2.55 μm. The emitting structure consists of two compressively strained GaInAsSb/GaSb-quantum wells placed within a lattice-matched AlGaAsSb waveguide. An average output power of more than 3 mW and a peak power of 38 mW are demonstrated at room temperature under pulsed operation. A cavity suppression element is used to prevent lasing at high current injection allowing emission in a broad spectrum with a full width at half maximum (FWHM) of 124 nm. The measured far-field of the SLD confirms a good beam quality at different currents. These devices open further development possibilities in the field of spectroscopy, enabling, for example, detection of complex molecules and mixtures of gases that manifest a complex absorption spectrum over a broad spectral range. https://doi.org/10.1063/1.5015974

Short wavelength infrared light sources emitting in the 2–3 μm wavelength range are very important for trace gas sensing, molecular spectroscopy, and chemical process monitoring.[1,2] In particular, light sources emitting at 2550 nm enable the detection of gases,[3] such as nitrous oxide (N_2O),[4] acetylene (C_2H_2),[5,6] carbon monoxide (CO),[3] and carbon dioxide (CO_2),[3] and the *in-situ* measurement of humidity (H_2O),[7] utilizing their spectroscopic fingerprint in this spectral range. Monitoring C_2H_2, CO_2, and N_2O is very important in the quest of reducing their detrimental impact on climate change and air pollution. Moreover, monitoring H_2O has important applications in optimizing different industrial processes, for example, in diagnosing the efficiency of a combustion engine. However, currently available light sources lack a suitable combination of performance in terms of attainable output power, spectral coverage, compactness, power consumption, and price. GaInAsSb/GaSb-based type-I quantum well (QW) lasers have shown good performance between 2 μm and 3 μm wavelengths.[8–10] However, since the typical wavelength coverage and tuning of a conventional diode laser are limited to a few nanometers,[11] broadband spectroscopy would require multiple diode lasers with different emission wavelengths and/or complicated external cavity elements for tuning to detect several gases simultaneously. On the other hand, superluminescent diodes (SLDs) exhibit broadband emission from single transverse mode ridge waveguides (RWGs), which is easy to collimate, focus, and couple into an optical fiber or a silicon waveguide. Despite these attractive features, the development of SLDs in spectral regions beyond 2 μm has seen little progress. This is partly due to relatively low spread of GaSb optoelectronics technology. Owing to the increased demand for spectroscopy, several groups have recently reported developments concerning SLDs with emission wavelengths up to 2.4 μm. The leading results are concerned with continuous wave (CW) operation of SLDs at room temperature (RT) with single transverse mode output powers up to 60 mW at 1.90 μm,[12] 40 mW at 2.05 μm, and 5 mW at 2.38 μm (Ref. 13) emission wavelengths. The severe power degradation at longer wavelengths is mainly due to the thermally activated Auger recombination process,[14] which increases with the wavelength, and is the dominant non-radiative recombination process at room temperature.[14,15] Moreover, the SLD carrier density in the active region increases monotonically with the current[16,17] rapidly increasing the Auger recombination rate as this is proportional to the third power of carrier density.[18]

In this letter, we report the development of a SLD at 2.55 μm, delivering mW-level average output power. In order to reduce the average carrier density, thus minimizing the carrier heating effects and the non-radiative Auger recombination, we use a pulsing scheme that allows us to reach mW-level average power while maintaining a high quality broadband spectrum. Operation at a high peak injection level without lasing, and hence high average power, is rendered possible by employing a cavity suppression (CS) element reported recently for the 2 μm wavelength.[12] High gain operation is particularly important for SLDs, as their output power is exponentially proportional to the modal gain.[19] The combination of the CS element and an advanced drive strategy allowed us to demonstrate an average output power of more than 3 mW at RT and a spectral full width at half maximum (FWHM) of 124 nm.

The epitaxial structure was grown on an n-GaSb substrate by molecular beam epitaxy. The structure comprised two 2% compressively strained $Ga_{0.54}In_{0.46}As_{0.13}Sb_{0.83}$ QWs placed between a lattice-matched $Al_{0.25}Ga_{0.75}As_{0.02}Sb_{0.98}$ waveguide with a total thickness of 540 nm. The compressive strain ensures the band alignment for type-I QWs with a 200 meV valence band offset.[20] The photoluminescence spectra measured for a separate QW-sample peaked at 2.55 μm. The active region was embedded in 2 μm thick p- and n-$Al_{0.6}Ga_{0.4}As_{0.04}Sb_{0.96}$

[a]Author to whom correspondence should be addressed: nouman.zia@tut.fi.

cladding layers. The doping levels were linearly graded from 2×10^{17} cm^{-3} to 2×10^{18} cm^{-3} in 500 nm thick cladding layers to minimize the free carrier absorption near the active region. The epitaxial structure was then capped with a 200 nm highly p-doped GaSb layer. The choice of the vertical structure was selected to provide a single mode waveguide in the growth direction and to maximize the modal gain provided by the QWs. Lateral optical confinement was ensured by employing a ridge waveguide (RWG) design to guide only the fundamental transverse mode. The single transverse mode operation of the ridge waveguide was first optimized by maximizing the confinement of the fundamental mode under the ridge with respect to the higher order transverse modes.[21] Transverse optical field profiles were obtained from solving the scalar Helmholtz eigenvalue problem with homogeneous Dirichlet boundary conditions using a finite difference scheme.[22] The boundaries were set far away so that they did not interfere with the solution validity. The epitaxial structure was optimized to ensure the high vertical confinement for the fundamental transverse mode than the other modes. The transverse mode confinement was optimized experimentally by selecting a ridge width and an etching depth combination to achieve a stable lobe free far-field profile and a kink-free light-current (L-I) characteristic.

In superluminescent diodes, the light reflection from the waveguide facets must be suppressed for low spectral modulations and broadband emission. This constraint requires a specific longitudinal design of the SLD waveguide. In general, cavity feedback suppression in SLDs is achieved by reducing the reflectivity of both[19] or one facet.[23] The most common approaches to prevent lasing inside the cavity are using ultra-low reflectivity antireflection (AR) coatings,[24] adding a highly active[25] or a passive absorber[26] section into the resonator, or tilting the waveguide with respect to the cavity facets.[19] An AR-coating can only decrease the reflectivity to 10^{-4} at a single wavelength; a multilayer AR-coating can reduce reflectivity over a relatively broad wavelength range, but the fabrication of multilayer AR-coatings makes the process difficult. A passive absorber section is not capable of completely suppressing the lasing inside the cavity. An active absorber section is a technique that is more effective, but it causes processing and biasing issues. A tilted waveguide is a rather simple approach, which can provide an extremely low facet reflectivity of below 10^{-5}. Recently,[12] we introduced a waveguide design in which the lasing was suppressed in 1.9 μm SLD by adding a CS element at one facet of a tilted RWG SLD. In the current report, we have tilted the RWG 8° with respect to the cavity facet, as the larger tilt angles suppress the lasing more effectively at longer wavelengths.[13] The length of the CS element is 90 μm, and the overall length of the device, including the RWG, is 2.5 mm. The choice of a long RWG has two main reasons: (1) it enables the high power operation as the SLD's single-pass gain depends exponentially on the length of the cavity and (2) it decreases the carrier density, which in turn lowers the Auger recombination. The schematic of our device is shown in Fig. 1, with the corresponding geometrical parameters in Table. I.

The preparation of the waveguides was done using UV-contact lithography to define the 5 μm wide ridge waveguides etched 1800 nm into the p-cladding using an inductively coupled reactive ion etch system with Cl_2/N_2-plasma chemistry. These waveguides were passivated with a 100 nm thick SiN-layer deposited using the plasma enhanced chemical vapour deposition (PECVD) technique. The SiN-layer was removed from the top of the waveguide in order to open a path to inject the current, and the p-side contact was deposited on the SiN and on the opened area. The p-side contact consisted of a Ti/Pt/Au-layer structure. To allow subsequent cleaving of high quality facets, the substrate was thinned down to 140 μm thickness and the n-side of the sample was metallized to produce the n-contact. For this step, we used an annealed Ni/Au/Ge/Au layer stack. Prior to testing, the chips were mounted on AlN-submounts with an epoxy-adhesive containing silver particles.

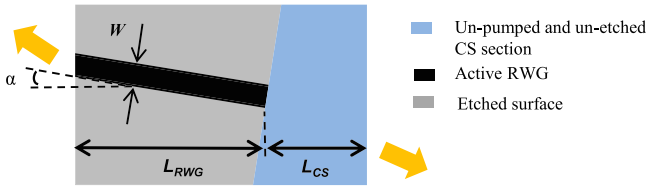

FIG. 1. Schematic drawing of the SLD waveguide geometry with the CS element on the right facet.

Output power characteristics were measured under pulsed injection with a constant pulse-width of 500 ns. We measured the peak and the average output powers by varying the current, duty cycle (DC), and heat sink temperature. Figure 2 shows the average and peak output powers versus the duty cycle for a set of different peak currents. At low currents (up to 400 mA) and up to 35% DC, the average power is nearly a quasi-linear function of DC without any clear sign of thermal degradation, as observed in Fig. 2(a). By increasing the current, device heating becomes significant and a thermal roll-over appears. For high currents, the thermal roll-over becomes sharper and the maximum average power shifts towards low duty cycles. The effect of the device heating can also be seen from the behavior of the peak power, as shown in Fig. 2(b). The peak power is high for higher currents at low duty cycles, which is not the case at high duty cycles. After the point of thermal roll-over, the peak power for the highest current (1400 mA) starts lagging the peak power for the lower current (1200 mA). This continues until the peak power for the lowest (300 mA) current becomes greater than for the highest current (1400 mA). For higher currents, the device heating starts to be more important and operating the device at higher duty cycles becomes more difficult.

Figure 3(a) shows the peak (solid line) and average powers (dashed-dotted line) of the SLD versus DC, at different temperatures, under a constant pulse injection of 1000 mA current. By decreasing the heat sink temperature from 30 °C to 10 °C, we have observed a shift in the DC, corresponding to the maximum average output power, from 14% to 26%. This shift in the duty cycle is due to a decrease in the

TABLE I. Parameters of the SLD geometry shown in Fig. 1.

RWG length L_{RWG} (μm)	2410
CS length L_{cs} (μm)	90
RWG width W (μm)	5
Tilt angle α (deg)	8

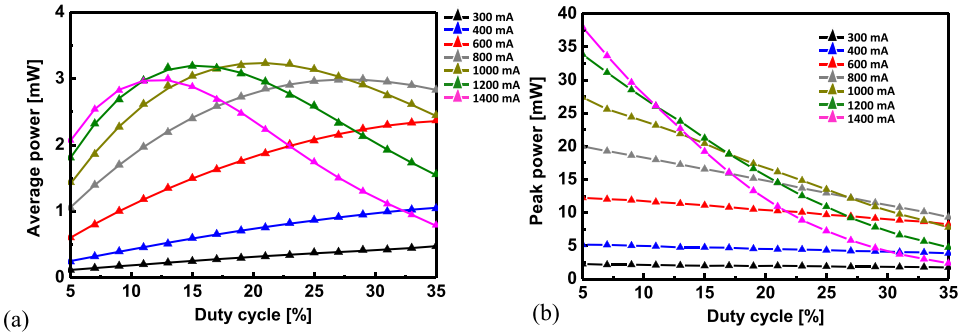

FIG. 2. (a) Average and (b) peak power versus duty cycle (DC) for a SLD driven under different peak currents. Pulse-width = 500 ns; heat sink temperature = 20 °C. Continuous lines are guides to the eye.

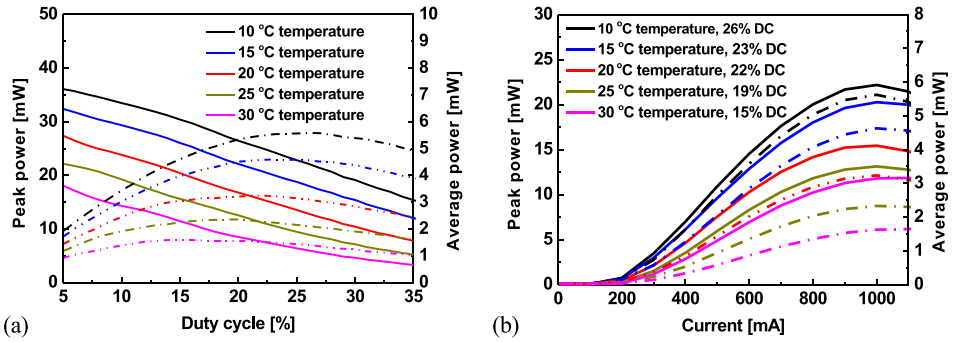

FIG. 3. (a) Peak (solid line) and average powers (dashed dotted line) versus duty cycle (DC) for a SLD driven under 1000 mA pulsed injection at different temperatures. (b) L-I characteristic of a SLD at different temperatures and at their corresponding maximum average power duty cycles. Pulse-width = 500 ns.

non-radiative Auger effect at low temperature, which permits the operations of the device at high DCs, and high average power, without early thermal roll-over. The light-current (L-I) characteristic curves at different temperatures and at their corresponding maximum DCs are shown in Fig. 3(b). The L-I curve shows that the SLD emits maximum average power around 6 mW at 10 °C and a corresponding peak power of 22 mW.

The emission spectra of the SLDs were measured using a monochromator with 0.4 nm resolution, under pulsed input current at 20 °C temperature. The FWHM of the spectrum measured at 600 mA current is 107 nm, which indicates that the device operates in the superluminescent regime. An increase in the current from 600 mA to 1200 mA changes the spectral FWHM from 107 nm to 124 nm, as shown in Fig. 4(a). This increase in the FWHM is due to the fact that the material gain bandwidth is growing faster than the square root of the effective device gain when the current density is increased.[27] The effect of temperature on the emission spectra is also examined and shown in Fig. 4(b). We can notice that an increase in temperature causes a red shift of 1.3 nm/°C in the spectral peak. This shift in the wavelength is attributed to the decrease in the bandgap with temperature, which for bulk GaInAsSb was estimated to be 1.5 nm/°C. The spectral broadening with the temperature increase is attributed to the gain broadening, as the carriers start to fill high-energy states due to thermal excitation.

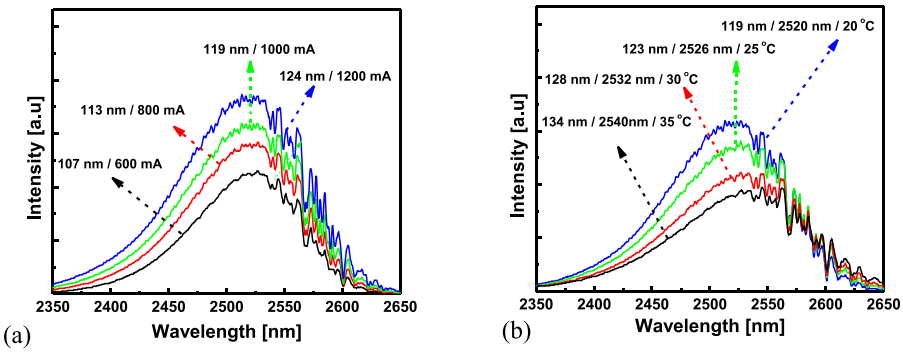

FIG. 4. SLD emission spectra measured under pulsed injection at (a) different currents and constant 20 °C heat sink temperature and (b) different temperatures and constant 1000 mA current. Pulse width = 500 ns; duty cycle = 5%. Arrows indicate FWHM at different injection currents in (a) and FWHM and peak wavelength at different heat sink temperatures in (b).

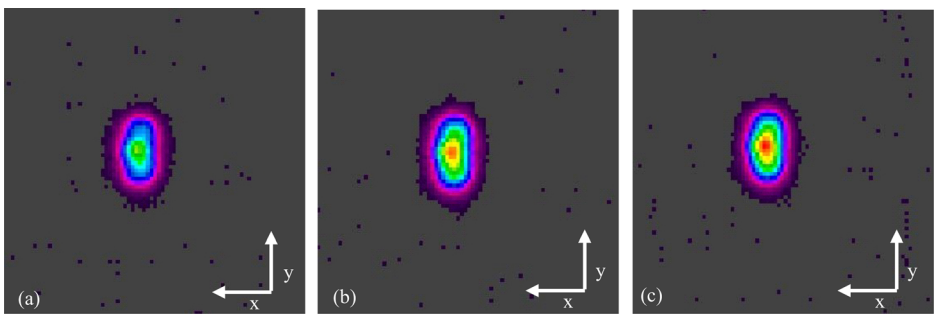

FIG. 5. Far field images acquired under pulse injection at (a) 600 mA, (b) 800 mA, and (c) 1000 mA. Here, the x-axis is parallel to the junction plane and the y-axis is in the growth direction.

We have also observed dips in the trailing edge of spectra, as seen in Fig. 4. These spectral dips are caused by the absorption characteristics of air, because spectral measurements were conducted in a non-vacuum environment.

In order to confirm the quality of an emitted beam from SLD, we measured the shape of the far-field distribution by using a beam profiling pyroelectric camera (Pyrocam III, Ophir). A collimated beam was incident on the pyroelectric camera, and the far-field was measured at different pulse injection currents. Beam profiles, shown in Fig. 5, for different levels of injection, reveal side-lobe-free intensity patterns across the current range indicating transverse single mode operation.

In conclusion, we report the development of a room-temperature mW-level broadband SLD at 2.55 μm using type-I GaInAsSb/GaSb-based compressively strained quantum wells. We used pulsed driving to minimize the carrier heating and thus the non-radiative Auger recombination rate. In particular, injection with sub-μs pulses leads to high peak gain values. In addition, for a high current injection and hence high output power, we employed a recently proposed cavity suppression element. SLD chips delivered up to 3.2 mW average power at 20 °C heat sink temperature, under 1 A peak current and 22% duty cycle (440 kHz repetition rate). A 10 K drop in the mount temperature increased the power up to about 6 mW. For a lower duty cycle of 5%, the SLDs delivered 38 mW of peak power. Devices exhibited wide emission spectra of 107 nm–124 nm, centered around 2526 nm–2540 nm depending on the operating temperature and current. The far-field of a device shows good beam quality at high currents without any side lobes. Such a level of output power, broad emission spectrum, and beam quality are instrumental for simpler implementation of spectroscopic systems in the field of trace gas sensing, molecular spectroscopy, and chemical process monitoring, where multiple emission lines over broad wavelength coverage need to be monitored simultaneously.

This work was carried out as a part of EU Horizon 2020 program MIREGAS (Grant Agreement No. 644192) and Academy of Finland Key project funding MIRELIGHT (Grant Agreement No. 644192). The authors would like to thank Mr. Riku Koskinen for his contribution in epitaxial growths and Ms. Maija Karjalainen for her contribution to device processing.

[1]P. Werle, "Spectroscopic trace gas analysis using semiconductor diode lasers," Spectrochim. Acta, Part A **52**(8), 805–822 (1996).
[2]M. E. Webber, J. Wang, S. T. Sanders, D. S. Baer, and R. K. Hanson, "*In situ* combustion measurements of CO, CO_2, H_2O and temperature using diode laser absorption sensors," Proc. Combust. Inst. **28**(1), 407–413 (2000).
[3]I. E. Gordon, L. S. Rothman, C. Hill, R. V. Kochanov, Y. Tan, P. F. Bernath, M. Birk, V. Boudon, A. Campargue, K. V. Chance *et al.*, "The HITRAN2016 molecular spectroscopic database," J. Quant. Spectrosc. Radiat. Transfer **203**(Supplement C), 3–69 (2017).
[4]H. Herbin, N. Picqué, G. Guelachvili, E. Sorokin, and I. T. Sorokina, "N_2O weak lines observed between 3900 and 4050 cm^{-1} from long path absorption spectra," J. Mol. Spectrosc. **238**(2), 256–259 (2006).
[5]N. Picqué, F. Gueye, G. Guelachvili, E. Sorokin, and I. Sorokina, "Time-resolved Fourier transform intracavity spectroscopy with a Cr^{2+}:ZnSe laser," Opt. Lett. **30**, 3410–3412 (2005).
[6]V. Girard, R. Farrenq, E. Sorokin, I. Sorokina, G. Guelachvili, and N. Picqué, "Acetylene weak bands at 2.5 μm from intracavity Cr^{2+}:ZnSe laser absorption observed with time-resolved Fourier transform spectroscopy," Chem. Phys. Lett. **419**, 584–588 (2006).
[7]C. S. Goldenstein, I. A. Schultz, R. M. Spearrin, J. B. Jeffries, and R. K. Hanson, "Scanned-wavelength-modulation spectroscopy near 2.5 μm for H_2O and temperature in a hydrocarbon-fueled scramjet combustor," Appl. Phys. B **116**(3), 717–727 (2014).
[8]C. Lin, M. Grau, O. Dier, and M.-C. Amann, "Low threshold room-temperature continuous-wave operation of 2.24–3.04 μm GaInAsSb/AlGaAsSb quantum-well lasers," Appl. Phys. Lett. **84**(25), 5088–5090 (2004).
[9]K. Kashani-Shirazi, K. Vizbaras, A. Bachmann, S. Arafin, and M. C. Amann, "Low-threshold strained quantum-well GaSb-based lasers emitting in the 2.5- to 2.7-μm wavelength range," IEEE Photonics Technol. Lett. **21**(16), 1106–1108 (2009).
[10]L. Shterengas, G. Kipshidze, T. Hosoda, J. Chen, and G. Belenky, "Diode lasers emitting at 3 μm with 300 mW of continuous-wave output power," Electron. Lett. **45**(18), 942–943 (2009).
[11]Q. Gaimard, M. Triki, T. Nguyen-Ba, L. Cerutti, G. Boissier, R. Teissier, A. Baranov, Y. Rouillard, and A. Vicet, "Distributed feedback GaSb based laser diodes with buried grating: A new field of single-frequency sources from 2 to 3 μm for gas sensing applications," Opt. Express **23**(15), 19118–19128 (2015).
[12]N. Zia, J. Viheriälä, R. Koskinen, A. Aho, S. Suomalainen, and M. Guina, "High power (60 mW) GaSb-based 1.9 μm superluminescent diode with cavity suppression element," Appl. Phys. Lett. **109**(23), 231102 (2016).
[13]K. Vizbaras, E. Dvinelis, I. Šimonytė, A. Trinkūnas, M. Greibus, R. Songaila, T. Žukauskas, M. Kaušylas, and A. Vizbaras, "High power continuous-wave GaSb-based superluminescent diodes as gain chips for widely tunable laser spectroscopy in the 1.95–2.45 μm wavelength range," Appl. Phys. Lett. **107**(1), 011103 (2015).
[14]T. D. Eales, I. P. Marko, B. A. Ikyo, A. R. Adams, S. Arafin, S. Sprengel, M.-C. Amann, and S. J. Sweeney, "Wavelength dependence of efficiency limiting mechanisms in type-I mid-infrared GaInAsSb/GaSb lasers," IEEE J. Sel. Top. Quantum Electron. **23**(6), 1–9 (2017).
[15]T. D. Eales, I. P. Marko, B. A. Ikyo, A. R. Adams, I. Vurgaftman, S. Arafin, S. Sprengel, M.-C. Amann, J. R. Meyer, and S. J. Sweeney, "Auger recombination in type I GaInAsSb/GaSb lasers and its variation with wavelength in the 2 to 3 μm range," in *Conference on Lasers and Electro-Optics Europe European Quantum Electronics Conference (CLEO/Europe-EQEC)*, 2017, p. 1.
[16]S. H. Oh, K. S. Kim, J. J. Ju, M.-S. Kim, K.-H. Yoon, D. K. Oh, Y.-O. Noh, and H.-J. Lee, "Tunable external cavity laser employing uncooled superluminescent diode," Opt. Express **17**(12), 10189–10194 (2009).
[17]M. B. Wootten, J. Tan, Y. J. Chien, J. T. Olesberg, and J. P. Prineas, "Broadband 2.4 μm superluminescent GaInAsSb/AlGaAsSb quantum well diodes for optical sensing of biomolecules," Semicond. Sci. Technol. **29**(11), 115014 (2014).
[18]L. A. Coldren, S. W. Corzine, and M. L. Mashanovitch, *Diode Lasers and Photonic Integrated Circuits*, 2nd ed. (Wiley, 2012).
[19]G. A. Alphonse, "Design of high-power superluminescent diodes with low spectral modulation," Proc. SPIE **4648**, 125–139 (2002).
[20]M. P. C. M. Krijn, "Heterojunction band offsets and effective masses in III-V quaternary alloys," Semicond. Sci. Technol. **6**(1), 27 (1991).
[21]T. Uusitalo, H. Virtanen, and M. Dumitrescu, "Transverse structure optimization of distributed feedback and distributed Bragg reflector lasers with surface gratings," Opt. Quantum Electron. **49**(6), 206 (2017).
[22]K. Bierwirth, N. Schulz, and F. Arndt, "Finite-difference analysis of rectangular dielectric waveguide structures," IEEE Trans. Microwave Theory Tech. **34**(11), 1104–1114 (1986).
[23]J. H. Liang *et al.*, "High-power high-efficiency superluminescent diodes with J-shaped ridge waveguide structure," in *Proceedings of the 14th Indium Phosphide and Related Materials Conference (Cat. No.02CH37307)*, 2002, pp. 119–122.
[24]N. Dutta and P. Deimel, "Optical properties of a GaAlAs superluminescent diode," IEEE J. Quantum Electron. **19**(4), 496–498 (1983).
[25]L. N. Kurbatov, S. S. Shakhidzhanov, L. V. Bystrova, V. V. Krapukhin, and S. I. Kolonenkova, Sov. Phys.-Semicond. **4**, 1739 (1971).
[26]A. Kafar, S. Stańczyk, R. Czernecki, M. Leszczyński, T. Suski, and P. Perlin, "Cavity suppression in nitride based superluminescent diodes," J. Appl. Phys. **111**(8), 083106 (2012).
[27]J. Park and X. Li, "Theoretical and numerical analysis of superluminescent diodes," J. Lightwave Technol. **24**(6), 2473 (2006).